

# Designing rigid carbon foams

Sora Park,<sup>1</sup> Kritsada Kittimanapun,<sup>2</sup> Jeung-Sun Ahn,<sup>1</sup> Young-Kyun Kwon <sup>\*</sup>,<sup>1</sup> and David Tománek <sup>†1</sup>

<sup>1</sup>*Department of Physics and Research Institute for Basic Sciences, Kyung Hee University, Seoul, 130-701, Korea*

<sup>2</sup>*Physics and Astronomy Department, Michigan State University, East Lansing, Michigan 48824-2320, USA*

(Dated: July 26, 2021)

We use *ab initio* density functional calculations to study the stability, elastic properties and electronic structure of  $sp^2$  carbon minimal surfaces with negative Gaussian curvature, called schwarzites. We focus on two systems with cubic unit cells containing 152 and 200 carbon atoms, which are metallic and very rigid. The porous schwarzite structure allows for efficient and reversible doping by electron donors and acceptors, making it a promising candidate for the next generation of alkali ion batteries. We identify schwarzite structures that act as arrays of interconnected quantum spin dots or become magnetic when doped. We introduce two interpenetrating schwarzite structures that may find their use as the ultimate super-capacitor.

PACS numbers: 81.05.Uw, 61.48.De, 73.22.-f, 71.20.-b, 62.25.-g

## I. INTRODUCTION

Nanostructured carbon has become an intensely researched topic since the discovery of the  $C_{60}$  molecule<sup>1</sup>, a previously unknown carbon allotrope. Most research has focussed on structures with zero or positive Gaussian curvature such as fullerenes, nanotubes and graphene<sup>2,3</sup>. Much less emphasis has been placed on structures with negative Gaussian curvature<sup>4,5,6,7,8,9,10,11,12,13,14,15,16,17,18</sup>, related to foams, which may be equally rigid and exhibit unusual electronic and magnetic properties. These systems, also called schwarzites, are space-filling contiguous structures formed of  $sp^2$  bonded carbon. They are unique in their ability to subdivide space into two disjoint, contiguous subspaces with labyrinthine morphology and the same infinite spatial extent.

Here we focus on two schwarzite structures with cubic unit cells containing between 152 and 200 carbon atoms. We also postulate a structure with 400 atoms per unit cell as a representative of a class of interpenetrating, but disconnected schwarzite lattices. Using *ab initio* density functional calculations, we determine the equilibrium structure as well as the elastic, electronic and magnetic properties of pristine and electron or hole doped schwarzites. Our calculations indicate the possibility of tuning the concentration of K and Cl atoms in order to achieve magnetic behavior. We find that the hole-doped  $C_{200}$  structure and similar systems may behave as an array of interconnected quantum spin dots. We discuss potential energy storage applications of schwarzites, such as next-generation electrodes for alkali ion batteries, and calculate the capacitance of two interpenetrating schwarzites, which may find their use as the ultimate

super-capacitor.

## II. COMPUTATIONAL METHOD

Our *ab initio* calculations are based on the density functional theory (DFT) within the local density approximation (LDA) and use the Ceperley-Alder exchange-correlation functional<sup>19</sup> as parameterized by Perdew and Zunger<sup>20</sup>. Interactions between valence electrons and ions are treated by norm-conserving pseudopotentials<sup>21</sup> with separable non-local operators<sup>22</sup>. Atomic orbitals with double- $\zeta$  polarization are used to expand the electron wave functions<sup>23,24</sup> with an energy cutoff of 210 Ry for the real-space mesh. We use 0.02 Ry as the confinement energy shift that defines the cutoff radii of the atomic orbitals. We sample the small Brillouin zone by 8  $k$ -points in order to represent the Bloch wave functions for the momentum-space integration. All geometries are optimized using the conjugate gradient method<sup>25</sup>, until none of the residual Hellmann-Feynman forces acting on any atom exceeds  $1.56 \times 10^{-3}$  Ry/ $a_B$ , where  $a_B$  is the Bohr radius.

## III. RESULTS

### A. Pristine schwarzite lattices

Previous theoretical studies addressed schwarzites with 24 (Ref. 9), 32 (Ref. 10), 48 (Ref. 11), 56 (Refs. 11,12), 72 (Ref. 12), 80 (Ref. 12), 168 (Refs. 13, 15), 192 (Refs. 14, 15), 200 (Ref. 11), 216 (Refs. 15, 16), and 224 (Ref. 17) atoms per unit cell, or related general morphology issues (Refs. 17, 18). We focus on two structures with a primitive ( $P$ ) minimal surface spanned by an underlying simple cubic lattice, which have not been studied previously and which contain 152 and 200 carbon atoms per unit cell. The  $C_{152}$  structure is depicted in Fig. 1(a) and the  $C_{200}$  structure in Fig. 1(b). The unit cells of

\*E-mail: ykkwon@khu.ac.kr

†E-mail: tomanek@pa.msu.edu; Permanent address: Physics and Astronomy Department, Michigan State University, East Lansing, Michigan 48824-2320, USA

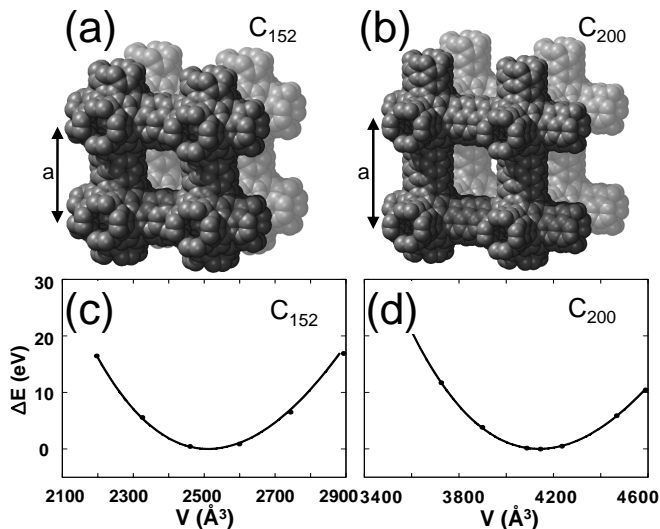


FIG. 1: Equilibrium geometry of *P* schwarzites with 152 (a) and 200 (b) carbon atoms per cubic unit cell with the lattice constant  $a$  and the volume  $V = a^3$ . Total energy change  $\Delta E$  as a function of  $V$  for the  $C_{152}$  (c) and  $C_{200}$  (d) schwarzites.

either schwarzite contain one “core” structure with  $O_h$  symmetry and a negative local Gaussian curvature. The six extremities of the cores are connected to neighboring cores by (4,4) carbon nanotube segments of various length to form a contiguous lattice. Negative Gaussian curvature is introduced by the presence of heptagons in the graphitic lattice. Our systems contain exactly 24 heptagons per unit cell in accordance with Euler’s theorem that, along with 24 hexagons, form the cores of the schwarzite. Each interconnect contains one nanotube unit cell with 8 hexagons in the  $C_{152}$  structure and two unit cells with 16 hexagons in the  $C_{200}$  structure.

To identify the equilibrium structure and elastic properties of the two schwarzite structures, we performed a series of structure optimizations at fixed unit cell volume. The total energy change  $\Delta E(V)$  with respect to the optimum structure is presented for the two structures in Figs. 1(c) and 1(d) along with Murnaghan function fits of our data. For the  $C_{152}$  schwarzite we find the binding energy  $E_{coh} = 10.50$  eV/atom at the equilibrium volume  $V_{eq} = 2515 \text{ \AA}^3$ , corresponding to the lattice constant  $a = 13.60 \text{ \AA}$ , gravimetric density  $\rho = 1.21 \text{ g/cm}^3$  and bulk modulus  $B = 111 \text{ GPa}$ . The less dense  $C_{200}$  schwarzite structure is slightly more stable with  $E_{coh} = 10.52$  eV/atom at  $V_{eq} = 4141 \text{ \AA}^3$ , corresponding to  $a = 16.06 \text{ \AA}$ , but has a smaller gravimetric density  $\rho = 0.96 \text{ g/cm}^3$  and bulk modulus  $B = 76.4 \text{ GPa}$ . The reduction of the binding energy with respect to the value of 10.88 eV/atom in a graphene monolayer is caused by the strain associated with curvature and is similar in value to carbon nanotubes. We find both structures to be substantially lighter than graphite ( $\rho = 2.27 \text{ g/cm}^3$ ) and diamond<sup>26</sup> ( $\rho = 3.54 \text{ g/cm}^3$ ). Also the bulk modulus of the stiffer  $C_{152}$  is about four times smaller than the

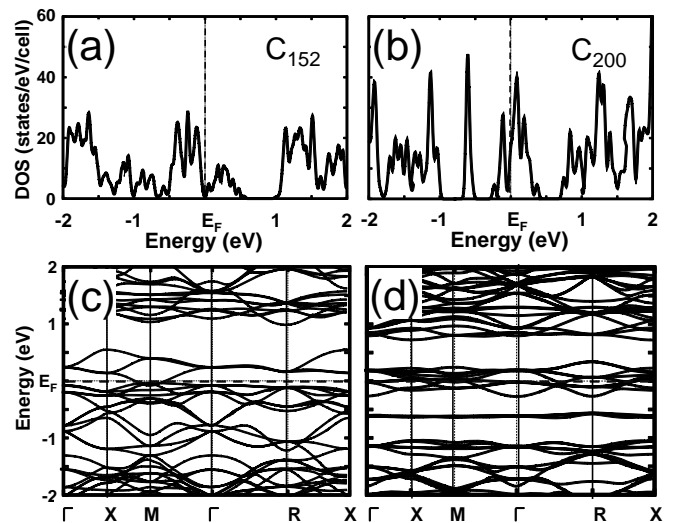


FIG. 2: Electronic structure of schwarzites. Density of states of the optimized schwarzite structures with unit cells containing 152 (a) and 200 (b) C atoms, smoothed with a Gaussian with the full width at half maximum of 0.03 eV. Corresponding band structure of the  $C_{152}$  (c) and  $C_{200}$  (d) schwarzites.

diamond value<sup>26</sup>  $B_{expt} = 442 \text{ GPa}$ .

To characterize the electronic properties of these schwarzites, we calculated their electronic density of states and band structure. The electronic densities of states of  $C_{152}$  and  $C_{200}$ , presented in Figs. 2(a) and 2(b), indicate that both structures are metallic. The origin of the individual peaks in the density of states can be traced back to the band structure graphs in Figs. 2(c) and 2(d). The schwarzites exhibit narrow band gaps above and, in the case of  $C_{200}$ , also below the Fermi level. Furthermore, as seen in Figs. 2(b) and 2(d), the  $C_{200}$  structure exhibits a 3-fold degenerate flat band about 0.62 eV below the Fermi level. Since in neither structure the Fermi level falls into a sharp peak, both structures are non-magnetic.

Besides the nonzero value of the density of states at  $E_F$  in the schwarzites we study, which makes them metallic, also the nature of those states is very important for the dielectric response of the system. Therefore, we plot the electron density associated with the frontier states at the Fermi level of  $C_{152}$  in Fig. 3(a) and that of  $C_{200}$  in Fig. 3(b). We find the frontier states to be highly delocalized in both systems. In the larger  $C_{200}$  schwarzite, we note that the frontier states have a node in the middle of the tubular interconnects between the cores, indicated by an arrow in Fig. 3(b). As seen in Fig. 3(c), which depicts the electron density of  $C_{152}$  associated with the  $\approx 0.8$  eV wide band mostly below the Fermi level, the corresponding states are distributed nearly uniformly across the structure. To understand the origin of the flat band in the  $C_{200}$  schwarzite 0.62 eV below the Fermi level, we present the associated electron density in Fig. 3(d). We may characterize this state as an array of non-interacting

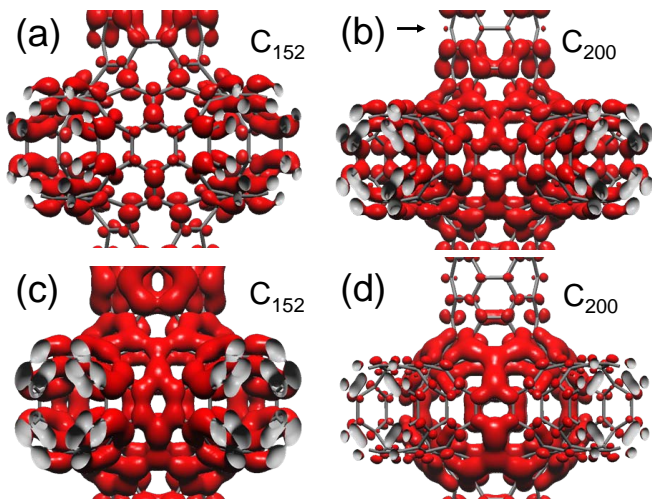


FIG. 3: (Color online) Electron densities in schwarzite structures containing 152 and 200 atoms per unit cell, presented as isodensity surfaces. Electron density associated with frontier states of  $C_{152}$  (a) and  $C_{200}$  (b) in the energy range  $E_F - 0.15$  eV  $< E < E_F + 0.15$  eV, presented at the isodensity value of  $10^{-2}$   $\text{\AA}^{-3}$ . (c) Electron density of  $C_{152}$  associated with states in the energy range  $E_F - 0.72$  eV  $< E < E_F + 0.10$  eV, presented at the isodensity value of  $10^{-2}$   $\text{\AA}^{-3}$ . (d) Electron density of  $C_{200}$  associated with the localized state near  $E_F - 0.62$  eV, presented at the isodensity value of  $10^{-4}$   $\text{\AA}^{-3}$ .

quantum dots centered in the negative Gaussian curvature regions at the cores of the  $C_{200}$  structure. We expect such a state to occur also in other schwarzite structures of the same type, which have larger unit cells due to longer tubular interconnects.

### B. Interpenetrating schwarzite lattices

The open space in the  $C_{152}$  and  $C_{200}$  structures, depicted in Figs. 1(a) and 1(b), can be filled by other atoms as external dopants. As we show in the following and depict in Figs. 4(a) and 4(b), the open space in the  $C_{200}$  schwarzite is wide enough and ideally suited to accommodate even an identical replica of the  $C_{200}$  schwarzite in an unstrained lattice.

In either schwarzite described in this manuscript, the tubular interconnects are composed of (4, 4) carbon nanotubes. As seen in Figs. 4(a) and 4(b), the closest approach distance between the sublattices occurs in the geometry depicted in the inset of Fig. 4(c), with two (4, 4) nanotube segments standing normal to each other. To estimate the optimum inter-wall separation, we calculated the inter-tube interaction in this geometry and plotted the data points along with a Morse function fit in Fig. 4(c). We found the optimum inter-tube distance to be  $d_{eq} = 7.8$   $\text{\AA}$ , corresponding to the closest inter-wall distance of 2.4  $\text{\AA}$ , somewhat smaller than the inter-layer distance in graphite. The corresponding distance

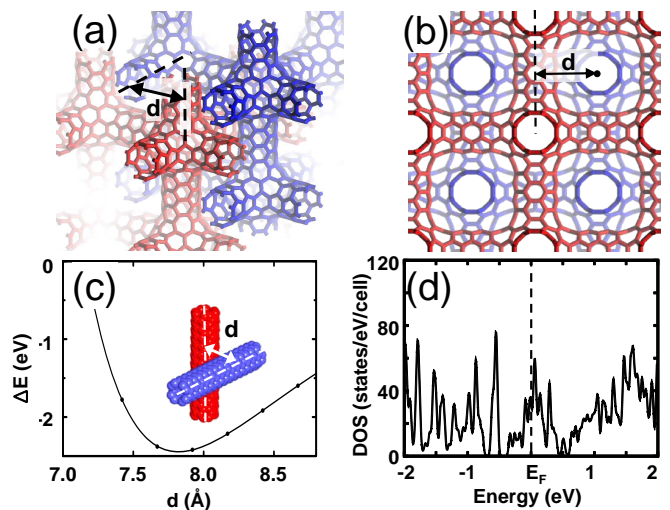


FIG. 4: (Color online) Equilibrium structure of two interpenetrating  $C_{200}$  schwarzite lattices, shown in Fig. 1(b), with 400 C atoms in total per unit cell, shown in perspective (a) and top (b) view. (c) Interaction energy between two (4, 4) nanotubes, with the geometry shown in the inset, representing the interaction between the tubular interconnects in the two interpenetrating  $C_{200}$  schwarzites. (d) Electronic density of states of the  $C_{400}$  schwarzite.

between adjacent tubular interconnects of the  $C_{200}$  substructures in  $C_{400}$ , as depicted in Figs. 4(a) and 4(b), is  $d = 8.00$   $\text{\AA}$ , which indeed is very close to the optimum inter-tube distance value  $d_{eq} = 7.8$   $\text{\AA}$ . Since the  $C_{400}$  schwarzite is structurally a superposition of two  $C_{200}$  schwarzite lattices, its gravimetric density is twice that of  $C_{200}$ , namely  $\rho = 1.92$  g/cm<sup>3</sup>. Also the bulk modulus of  $C_{400}$ ,  $B = 153$  GPa, is twice that  $C_{200}$ , which is about one third of the diamond value.

As the electronic density of states of the  $C_{200}$  sublattices, also that of the  $C_{400}$  schwarzite, shown in Fig. 4(d), has a large density of states at the Fermi level, indicating a metallic system. Similar to  $C_{200}$ , also  $C_{400}$  has a narrow band about 0.6 eV below  $E_F$ , associated with a lattice of very weakly coupled quantum dots. Careful comparison of Figs. 2(b) and 4(d) indicates that the central band around  $E_F$  becomes wider in the  $C_{400}$  lattice in comparison to the  $C_{200}$  lattice. This band broadening is accompanied by a corresponding narrowing of the band gaps above and below this central band.

### C. Intercalated schwarzites

As mentioned above, the empty space delimited by the schwarzite minimal surface can accommodate intercalant ions in order to shift the Fermi level. We consider K as a model donor that has been used widely in graphite intercalations compounds (GICs)<sup>27</sup>. Due to its highest electronic affinity in the periodic table<sup>26</sup> of 3.61 eV, we choose Cl as a model acceptor.

As in the previous subsection, we focus on the  $C_{200}$  schwarzite structure. To maximize charge transfer between the intercalant atoms and the schwarzite lattice, we place one K or Cl atom in the center of each core of the schwarzite. To estimate the charge transfer between the intercalants and the schwarzite, we performed a Mulliken population analysis and, alternatively, integrated the total electron density within a sphere surrounding the intercalant ion. We found the Mulliken charge on K to be  $+0.96e$  and that on Cl to be  $-0.42e$ . Electron density integration around the intercalant within schwarzite only makes sense up to the size of the cavity inside the core structure. Considering a sphere with a radius of  $R = 2.4 \text{ \AA}$  around Cl yields 7.00 valence electrons in case of an isolated atom and 7.42 valence electrons in case of  $Cl@C_{200}$ . Since the atomic radius of K is much larger, an isolated atom contains only 0.56 valence electrons within a sphere with  $R = 2.4 \text{ \AA}$ . Upon intercalation, in  $K@C_{200}$ , it loses almost all of the valence charge, so that only 0.01 valence electrons remain within this sphere.

By subtracting the total energy of  $C_{200}$  and the isolated atom A from that of  $A@C_{200}$ , where  $A=K$  or  $Cl$ , we found that the K atom stabilizes the unit cell by 2.080 eV, whereas the Cl atom provides a smaller stabilization by 0.636 eV per unit cell, partly due to the smaller charge transfer.

The ability to efficiently transfer most of the valence charge from the alkali atom to the graphitic structure is used currently in Li ion batteries, where Li is intercalated in-between graphene layers in graphite, causing an  $\approx 30\%$  expansion in the direction normal to the graphene layers. Repeating expansion and contraction during charge/discharge cycles is known to reduce the lifetime of alkali ion batteries, as it causes structural rearrangement of the grains and eventually blocks diffusion pathways. No such adverse effects should occur in the rigid, but still conductive schwarzite structures, which may yield a new generation of advanced alkali ion batteries. As a different potential application of doped schwarzites, we wish to mention their potential for hydrogen storage, similar to Ca doped  $C_{60}$  crystals that proved to store reversibly molecular hydrogen<sup>28</sup> up to 8.4%(wt).

As suggested by the smaller amount of charge transferred from the  $C_{200}$  schwarzite to Cl ions, the effect of acceptor intercalation is much smaller than that of donor intercalation. Nevertheless, hole doping should make it possible to shift  $E_F$  down. Especially interesting appears the possibility to move the Fermi level into the region of the threefold degenerate flat band. Partial occupation of the band is expected to change the system to a ferromagnet with a magnetic moment per unit cell up to  $6\mu_B$ . To determine the necessary amount of doping, we estimated the occupied portion of the band near  $E_F$  to carry 6 electrons. Combining this with the fact that the flat band also contains 6 electrons, we conclude that hole doping  $C_{200}$  with 7 – 11 electrons per unit cell should, assuming that the rigid band model applies, move the Fermi level into the region of the flat band. Using the

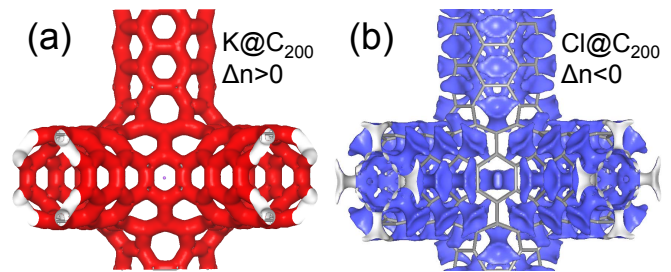


FIG. 5: (Color online) Electron density difference  $\Delta n(A@C_{200}) = n_{tot}(A@C_{200}) - n_{tot}(A) - n_{tot}(C_{200})$ , providing insight into the charge flow in the  $C_{200}$  schwarzite following intercalation with  $A = K, Cl$  atoms. (a)  $\Delta n(K@C_{200})$  at the isodensity value  $+0.04 \text{ \AA}^{-3}$ . (b)  $\Delta n(Cl@C_{200})$  at the isodensity value  $-0.04 \text{ \AA}^{-3}$ .

charge transfer estimated for one Cl atom in  $C_{200}$ , this could be achieved by intercalating between  $\approx 10 - 30$  Cl atoms per unit cell. Using interatomic distances from free  $Cl_2$ , we believe that in the optimum case,  $Cl_6$  clusters could be accommodated in the cores. Assuming that also each tubular interconnect could accommodate up to two Cl atoms, the Cl doped system should barely reach the criterion of partly depleting the initially flat band by Cl doping, causing ferromagnetism to occur.

To get an impression of how uniformly the transferred charge is distributed across the schwarzite lattice, we plot in Fig. 5(a) the distribution of the excess electron density in  $K@C_{200}$  and in Fig. 5(b) the corresponding distribution of the deficient electron density in  $Cl@C_{200}$ . Since both ions are well separated from the schwarzite lattice, we find that the transferred charge is distributed rather uniformly across the schwarzite in both cases.

Also the two interpenetrating  $C_{200}$  lattices, forming the  $C_{400}$  schwarzites, can be differentially doped, one with K and the other with Cl atoms, giving a net positive charge to one and a net negative charge to the other sublattice, similar to a capacitor. We superposed the  $K@C_{200}$  and  $Cl@C_{200}$  lattices and found a net stabilization with respect to separated  $K@C_{200}$  and  $Cl@C_{200}$  doped schwarzites of  $-15.735 \text{ eV}$ . Similar to the doped sublattices, the Mulliken population analysis indicates that the net charge on K is close to  $+0.70e$  and that on Cl is close to  $-0.42e$ . The opposite charges are then accommodated in the adjacent  $C_{200}$  substructure.

In the following we will estimate the capacitance of the schwarzite structure per  $1 \text{ cm}^3$  volume. The capacitance of a parallel-plate capacitor of area  $A$  and interplate distance  $d$ , defining the volume  $V = Ad$ , is given by  $C = \epsilon_0 A/d$  in SI units. For the sake of reference, an idealized capacitor with  $V = 1 \text{ cm}^3$ , formed by a graphene bilayer with  $d = 0.335 \text{ nm}$ , would have the area  $A = 3.0 \times 10^3 \text{ m}^2$  and a capacitance of 79.3 F. In the unit cell of the  $C_{400}$  schwarzite with the volume  $V = 4.141 \text{ nm}^3$ , 200 carbon atoms are associated with one electrode. With an estimated area per carbon atom of  $2.62 \text{ \AA}^2$ , same as in graphene, we estimate that

the area of one electrode per  $\text{cm}^3$  schwarzite should be  $1.3 \times 10^3 \text{ m}^2$ . Assuming furthermore the same average interlayer distance as in a graphene bilayer, we estimate the capacitance of the  $\text{C}_{400}$  schwarzite to be 34.3 F per  $\text{cm}^3$  material.

As an independent way to estimate the capacitance of the  $\text{C}_{400}$  schwarzite, we carefully inspected the total energy differences between neutral  $\text{C}_{200}$  and  $\text{C}_{400}$  systems, as well as the total energies of  $\text{K}@\text{C}_{200}$ ,  $\text{Cl}@\text{C}_{200}$  and  $\text{C}_{400}$  containing both K and Cl. The latter structure, which contains one positively and one negatively charged  $\text{C}_{200}$  minimal surface per unit cell, is a superposition of  $\text{K}@\text{C}_{200}$  and  $\text{Cl}@\text{C}_{200}$ . The stabilizing interaction between the charged  $\text{C}_{200}$  substructures of 15.735 eV is partly due to the chemical interaction between the two electrodes, which we estimated to be 15.464 eV per unit cell in the pristine system. We assign the remaining part of the interaction energy, 0.271 eV, to be the energy associated with the electric field between the capacitor plates. To understand the meaning of this energy gain, we consider two parallel plate electrodes carrying constant charges  $+Q$  and  $-Q$ , approaching from infinity to form a parallel-plate capacitor of capacitance  $C$ , thereby gaining the energy  $\Delta U = Q^2/(2C)$ . Considering  $\Delta U = 0.271 \text{ eV}$  and  $|Q| = 0.42e$ , the smaller of the charges transferred between the intercalant atoms and the neighboring electrodes, we can estimate the capacitance  $C$  per unit cell and the corresponding value in the bulk  $\text{C}_{400}$  schwarzite material, which turns out to be 12.6 F per  $\text{cm}^3$ .

We would like to point out that the above capacitance values are based on rough approximations and thus should be considered as order-of-magnitude estimates. Still, we are pleased that our estimate based on total energy differences in the intercalated system lies close to the estimate based on area and inter-plate distance. In

any case, the estimated capacitance exceeds that of nowadays' capacitors by several orders of magnitude. Should a material close to the postulated  $\text{C}_{400}$  schwarzite ever be synthesized, we must also consider the need to connect the two interpenetrating sublattices to two leads, which will be a nontrivial task. We also need to point out that the close proximity of the two electrodes in the schwarzite material promotes tunneling, which would eventually discharge the electrodes over time. Still, the expected capacitance of tens of Farads per cubic centimeter is an appealing prospect.

In summary, we studied the stability, elastic properties and electronic structure of  $sp^2$  carbon periodic minimal surfaces with negative Gaussian curvature, called schwarzites, using *ab initio* density functional calculations. Our studies of two primitive minimal surfaces, spanned by an underlying simple cubic lattice with 152 and 200 carbon atoms, indicate that these systems are very stable, rigid, and electrically conductive. The porous schwarzite structure allows for efficient and reversible doping by intercalation of electron donors or acceptors. We identified systems that should act as arrays of interconnected quantum spin dots or, when doped, exhibit ferromagnetic behavior. We also introduce two interpenetrating schwarzite structures as an unusual system that may find its use as the ultimate super-capacitor.

We acknowledge contributions of Thomas Moore and Daniel Enderich to the visualization of schwarzite structures. DT was supported by the International Scholar fellowship at Kyung Hee University and funded by the National Science Foundation under NSF-NSEC grant 425826 and NSF-NIRT grant ECS-0506309. YK was supported by NRF of Korea grant KRF-2009-0074951.

- 
- <sup>1</sup> H. W. Kroto, J. R. Heath, S. C. O'Brien, R. F. Curl, and R. E. Smalley. *Nature*, 318:162–163, 1985.
- <sup>2</sup> M.S. Dresselhaus, G. Dresselhaus, and P.C. Eklund. *Science of Fullerenes and Carbon Nanotubes*. Academic Press, San Diego, 1996.
- <sup>3</sup> A. Jorio, M.S. Dresselhaus, and G. Dresselhaus, editors. *Carbon Nanotubes: Advanced Topics in the Synthesis, Structure, Properties and Applications*. Number 111 in Topics in Applied Physics. Springer, Berlin, 2008.
- <sup>4</sup> A. L. Mackay.
- <sup>5</sup> R. Blinc, D. Arcon, P. Umek, T. Apih, F. Milia, and A. V. Rode. *Phys. Status Solidi B*, 244:4308–4310, 2007.
- <sup>6</sup> T. Petersen, I. Yarovsky, I. Snook, D. G. McCulloch, and G. Opletal. *Carbon*, 42:2457–2469, 2004.
- <sup>7</sup> Z. X. Wang, L. P. Yu, W. Zhang, J. G. Han, Z. Y. Zhu, G. W. He, Y. Chen, and G. Hu. *Chem. Phys. Lett.*, 380:78–83, 2003.
- <sup>8</sup> K. M. Merz, R. Hoffmann, and A. T. Balaban. *J. Am. Chem. Soc.*, 109:6742–6751, 1987.
- <sup>9</sup> Michael O'Keeffe, Gary B. Adams, and Otto F. Sankey. *Phys. Rev. Lett.*, 68:2325–2328, 1992.
- <sup>10</sup> R. B. Kusner, P. M. Lahti, and C. P. Lillya. *Chem. Phys. Lett.*, 241:522–527, 1995.
- <sup>11</sup> Ming-Zhu Huang, W. Y. Ching, and Thomas Lenosky. *Phys. Rev. B*, 47:1593–1606, 1993.
- <sup>12</sup> S. Gaito, L. Colombo, and G. Benedek. *Europhys. Lett.*, 44:525–530, 1998.
- <sup>13</sup> David Vanderbilt and J. Tersoff. *Phys. Rev. Lett.*, 68:511–513, 1992.
- <sup>14</sup> A. L. Mackay and H. Terrones. *Nature*, 352:762, 1991.
- <sup>15</sup> Rob Phillips, David A. Drabold, Thomas Lenosky, Gary B. Adams, and Otto F. Sankey. *Phys. Rev. B*, 46:1941–1943, 1992.
- <sup>16</sup> T. Lenosky, X. Gonze, M. Teter, and V. Elser. *Nature*, 355:333–335, 1992.
- <sup>17</sup> Elena R. Margine, Aleksey N. Kolmogorov, Dragan Stojkovic, Jorge O. Sofo, and Vincent H. Crespi. *Phys. Rev. B*, 76:115436, 2007.
- <sup>18</sup> Humberto Terrones and Mauricio Terrones. *Carbon*, 36:725–730, 1998.

- <sup>19</sup> D. M. Ceperley and B. J. Alder. *Phys. Rev. Lett.*, 45:566, 1980.
- <sup>20</sup> J. P. Perdew and A. Zunger. *Phys. Rev. B*, 23:5048, 1981.
- <sup>21</sup> N. Troullier and J. L. Martins. *Phys. Rev. B*, 43:1993, 1991.
- <sup>22</sup> L. Kleinman and D. M. Bylander. *Phys. Rev. Lett.*, 48:1425, 1982.
- <sup>23</sup> D. Sánchez-Portal, P. Ordejón, E. Artacho, and J. M. Soler. *Int. J. Quantum Chem.*, 65:453, 1997.
- <sup>24</sup> J. M. Soler, E. Artacho, J.D. Gale, A. García, J. Junquera, P. Ordejón, and D. Sánchez-Portal. *J. Phys.: Condens. Matter*, 14:2745–2779, 2002.
- <sup>25</sup> M. R. Hestenes and E. Stiefel. *J. Res. Natl. Bur. Stand.*, 49:409–436, 1952.
- <sup>26</sup> Charles Kittel. *Introduction to Solid State Physics*. Wiley, New York, eighth edition, 2005.
- <sup>27</sup> M. S. Dresselhaus and G. Dresselhaus. *Adv. Phys.*, 51:1–186, 2002.
- <sup>28</sup> Mina Yoon, Shenyuan Yang, Christian Hicke, Enge Wang, David Geohegan, and Zhenyu Zhang. *Phys. Rev. Lett.*, 100:206806, 2008.